Wideband Channel Measurements and Temporal-Spatial Analysis for Terahertz Indoor Communications

Ziming Yu[1], **Yi Chen**[2], **Guangjian Wang**[1], **Weijun Gao**[2], and **Chong Han**[2]

[1] Huawei Technologies Co., Ltd, China. Email: {yuziming, wangguangjian}@huawei.com
[2] Shanghai Jiao Tong University, China. Email: {yidoucy, gaoweijun, chong.han}@sjtu.edu.cn

***Abstract*—Terahertz communications are envisioned as a key technology for beyond 5G wireless systems, owing to its unprecedented multi-GHz bandwidth. In this paper, a wideband channel measurement between 130 GHz and 143 GHz is investigated in a typical meeting room for future THz wireless communication access networks. Directional antennas are utilized for resolving the MPCs in the angular domain. With careful system calibration that eliminates system errors and antenna effects, the channel transfer function is developed. Furthermore, ray-tracing techniques are utilized to post-process the measured data. In light of the measurement results, physical parameters and insights in the THz indoor channel are comprehensively analyzed, including the line-of-sight path loss, power-delay-angular profiles, temporal and spatial features, and correlations among THz multipath characteristics.**

***Index Terms*—Terahertz communications, Channel measurement, Channel characterization.**

I. Introduction

In the past few decades, wireless data traffic has witnessed exponential growth and brings an increasing demand for high-speed wireless communication. New spectral bands will be required to support the high data rate for future wireless applications [1]. Currently, wireless local area networks (WLAN) techniques, i.e., 802.11ad protocol and fifth-generation (5G) mobile networks, have opened up the millimeter-wave (mmWave) spectrum (10-100 GHz) for seeking wider bandwidth and higher data rates. However, their data rates are still limited within 10 Gbps. Meanwhile, the Terahertz (THz) (0.1-10 THz) band, which is capable of providing dozens and hundreds of gigahertz (GHz) continuous spectrum bands, is envisioned as one of the promising spectrum bands to enable ultra-broadband communications. The use of THz band can address the spectrum scarcity and capacity limitations of current wireless systems, and THz communications are foreseen to come into reality in the very near future. Specifically, 140 GHz band is the first spectral window to penetrate into the THz band, with mature electronic-based device technologies.

Though the THz band is attractive, one fundamental challenge is to measure, analyze, and model the THz electromagnetic wave propagation and channel characteristics [2]. From the literature, a number of channel measurement campaigns at THz frequencies have been reported for short-distance indoor scenarios [3]–[6], and outdoor vehicular communications [7]–[9]. On one hand, indoor channel measurement campaigns focus on the short-range, for example, on a desk [4] and on a computer motherboard [6]. On the other hand, the room-scale studies in [3], [5] consist of very few transmitter-receiver (Tx-Rx) pairs in a living room or office room. Therefore, an extensive channel measurement with various Tx and Rx positions in a meeting room environment for THz frequencies is still missing. Furthermore, thorough channel characterization on the THz propagation features is not well captured, which includes K-factor, sparsity, temporal and spatial dispersion, correlation of multipath features, among others.

In this paper, we present a wideband channel measurement campaign at 130-143 GHz in a typical meeting room. With a fixed Tx, multipath measurements are conducted at ten different receiver positions. Directional antennas are equipped at Tx and Rx to resolve multipath components (MPCs) in the angular domain. To assist post-processing of the measured data, we invoke ray-tracing techniques to simulate the propagation in the same geometry, and develop a multipath component distance (MCD) matching algorithm to trace the propagation path of a measured MPC. In light of the measurement results, we analyze the physical parameters and insights in the THz indoor channel. Specifically, the measured path loss of line-of-sight (LoS) path is validated with theoretical computation results. Moreover, the power-delay-angular profiles (PDAPs) are presented to reveal the multipath channel sparsity in the THz indoor environment, and significance of reflection over walls. Furthermore, temporal and spatial features including the K-factor, delay and power spreads are analyzed. Finally, a correlation matrix is formulated to analyze the dependence among the multipath characteristics of the THz indoor channel, e.g., Tx-Rx separation distance, number of MPCs, K-factor, delay spread, and angular spread.

The remainder of this paper is organized as follows. In Sec. II, we describe the channel measurement campaign and post-processing of measured data. We present the channel measurement results and more importantly, analyze the channel characteristics in Sec. III. Finally, the paper is concluded in Sec. IV.

978-1-7281-7440-2/20/$31.00 ©2020 IEEE

II. Channel Measurement Campaign

Before presenting the results of the channel measurement and the analysis of the THz indoor channel characteristics, we first detail the descriptions of the channel measurement campaign to help them better understood. In this section, we will introduce the THz measurement system, indoor environment, and measurement deployment. At last, we will show how we calibrate and post-process the measurement data.

The measurement platform consists of a 140 GHz transmission system and a vector network analyzer (VNA). The signal produced by VNA is up-converted to the frequency band from 130 to 140 GHz, and S parameters are recorded. As a result, the time domain resolution, Δt, is 76.9 ps, and we can resolve the two paths the difference between the path lengths of which is larger than 2.3 cm. The recorded points in the frequency domain, which we call the sampling points, are 1301, which corresponds to the sampling interval, Δf, of 10 MHz. The maximum excess delay, τ_m, is calculated as 100 ns. Accordingly, the maximum detected path length, L_m, of 30 m, which is long enough for an indoor channel measurement.

The antennas at Tx and Rx are horn antennas. The antenna at Tx produces an antenna gain of 15 dBi with the half-power beamwidth (HPBW) of 30° at 140 GHz. The HPBW of the antenna at Rx is 10°, which is one-third of that at Tx for high spatial resolution, and its antenna gain is 25 dBi. The two antennas are mounted on two rotation units and rotated by step motors, respectively. The detailed parameters of the platform are summarized in Table I.

TABLE I
MEASUREMENT PARAMETERS

Parameter	Symbol	Value
Start frequency	f_{start}	130 GHz
End frequency	f_{end}	143 GHz
Bandwidth	B_w	13 GHz
Sampling points	N	1301
Sampling interval	Δf	10 MHz
Average noise floor	P_N	-120 dBm
Test signal power	P_{in}	1 mW
HPBW of transmitter	$HPBW^{Tx}$	30°
HPBW of receiver	$HPBW^{Rx}$	10°
Antenna gain at Tx	G_{t}	15 dBi
Antenna gain at Rx	G_{r}	25 dBi
Time domain resolution	Δt	76.9 ps
Path length resolution	ΔL	2.3 cm
Maximum excess delay	τ_m	100 ns
Maximum path length	L_m	30 m

A. Measurement Environment and Deployment

We carried out the channel measurement in a typical meeting room with an area of 10.15 m × 7.9 m and a ceiling height of 4 m. In the meeting room, a 4.8 m × 1.9 m desk with a height of 0.77 m is placed in the center, and a number of chairs are around the desk, as shown in Fig. 1(a). In addition, two TVs are closely placed and parallel to a wall. The material of one wall is glass, while the other three walls are lime walls.

(a) Meeting room for THz channel measurements.

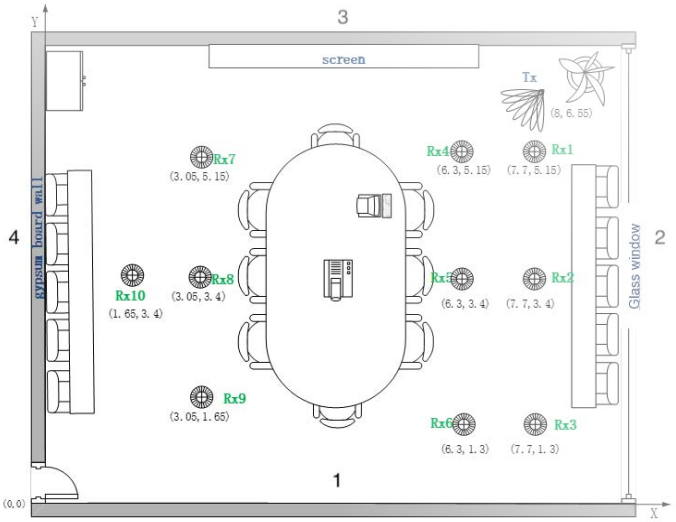

(b) Overview of the meeting room and measurement deployment.

Fig. 1. The meeting room layout and measurement deployment.

We notice that the maximum detected path length is 30 m, which is three times the largest dimension of the meeting room. As a result, the reflected paths with at least three-order reflection can be detected in our measurement.

To simulate the indoor scenario, Tx with HPBW of 30° is fixed as an AP at a corner of the meeting room. Its height is set to be 2 m, which is higher than the Rx, which is regarded as UE, the height of which is 1.4 m. The wider HPBW for Tx guarantees the coverage of the target UE and the smaller HPBW for Rx of 10° provides high spatial resolution for spatial-domain channel measurement. In our measurement deployment, 10 measured positions of Rx are distributed in the meeting room, some of which are near the Tx (Rx1 and Rx4) while some of which are far from the Tx and close to the corner (Rx3, Rx7 and Rx9), as depicted in the top view of the meeting room (Fig. 1(b)). The Euclidean distance between Tx and Rx ranges from 1.8 m to 7.3 m. For each measurement point, the main beam of Tx is directed to the Rx. Accordingly, Rx will scan the in the azimuth domain with the spatial resolution of 10°.

B. System Calibration and Data Post-processing

To eliminate the effects of the measurement system and antennas, we calibrate the S21 parameters recorded from VNA after the measurement campaign. The first step is to obtain the

S21 of the measurement system. For this purpose, we remove the transmit and receive antennas connected to the TX and Rx radiofrequency (RF) fronts and connect the RF fronts with a THz attenuator, the channel transfer function of which, H_{att}, we already know. By sweeping the spectrum band, we record the S21 parameter for calibration, S_{21}^{cal}, which is given by,

$$S_{21}^{\text{cal}} = H_{\text{sys}} \cdot H_{\text{att}}, \tag{1}$$

where H_{sys} is the channel transfer function of the measurement system. By using the recorded, S_{21}^{cal}, and the antenna gains of Tx and Rx, G_t and G_r, we can calibrate the S21 parameter which we measure for each measurement point, S_{21}^{mea}, and obtain the channel transfer function without the effects of the measurement system and antennas, H, as

$$H(f) = \frac{S_{21}^{\text{mea}} \cdot H_{\text{att}}}{S_{21}^{\text{cal}} \cdot G_t \cdot G_r}. \tag{2}$$

After the system calibration, we operate IDFT on the calibrated channel transfer function, $H(f)$, to compute the channel impulse response, $h(\tau)$. Finally, we conduct ray-tracing algorithm in the same environment as in the measurement campaign to help understand the propagation of the measured MPCs.

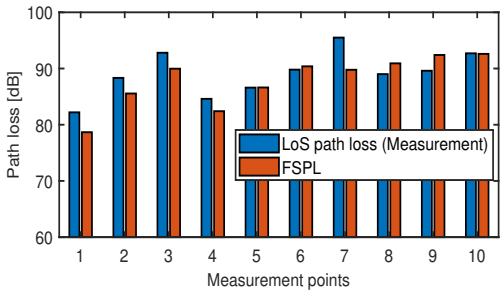

Fig. 2. Comparison between measured LoS path loss and FSPL.

III. THz Channel Characterization and Analysis

In this section, we thoroughly analyze the THz indoor channel characteristics, from the perspectives of path loss of the LoS path, MPCs reflection characteristics, and the temporal and spatial multipath characteristics. Properties and physical parameters revealed in this work are guidelines for THz communication design.

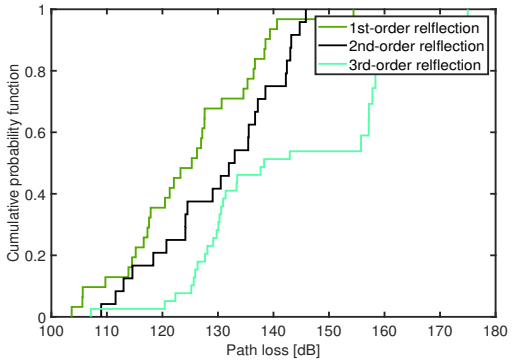

Fig. 3. CDF of reflected paths.

A. Path Loss of LoS Path

When the directional antennas between Tx and Rx are pointed to each other, the MPCs effect becomes insignificant, and the LoS path is dominant in the THz band. The path loss of an LoS path is the negative number of its S21 parameter averaged over the measurement spectrum band when the Tx and Rx are directed to each other. As depicted in Fig. 2, the path loss values of LoS path at all the receivers are compared with the free-space path loss (FSPL) calculated by Friss' law,

$$\text{FSPL [dB]} = -20\log_{10}\left(\frac{c}{4\pi f d}\right) \tag{3}$$

where c denotes the light speed, f is the carrier frequency and d is the separation distance between Tx and Rx.

By comparison, we observe the measured path loss coincides well with the FSPL computation. This demonstrates that the calibration works properly to suppress system errors and antenna gain effects. However, an average deviation of 2 dB arises, due to the following reasons. First, when the receiver is close to the Tx, for instance, Rx1, Rx2, and Rx4, the measured values of LoS path loss are higher than the results in (3). This is due to antenna misalignment at the elevation plane, where the eAoA exceeds the largest eAoA scanned in the measurement. Second, constructive effects caused by the reflected path from the desk results in a smaller path loss at Rx8 and Rx9. Third, the largest path loss difference 6.55 dB appears at Rx7, since its LoS path is partially obstructed by a chair.

TABLE II
Reflections of MPCs for all the Rxs

RX	Number of MPCs	1st-order reflection		2nd-order reflection		3rd-order reflection		$\frac{P_{\text{Wall}}}{P_{\text{Obstacle}}}$
		Wall	Obstacle	Wall	Obstacle	Wall	Obstacle	
1	8	1	3	2	0	2	0	1.10
2	11	3	1	4	1	2	0	9.08
3	11	3	3	4	0	1	0	9.08
4	14	3	3	3	1	3	1	8.14
6	8	3	0	3	0	1	1	618.65
7	8	2	0	2	0	2	2	13.13
8	6	2	0	1	1	2	0	9.58
9	5	2	0	1	0	2	0	Inf
10	5	2	0	1	0	0	2	0.95

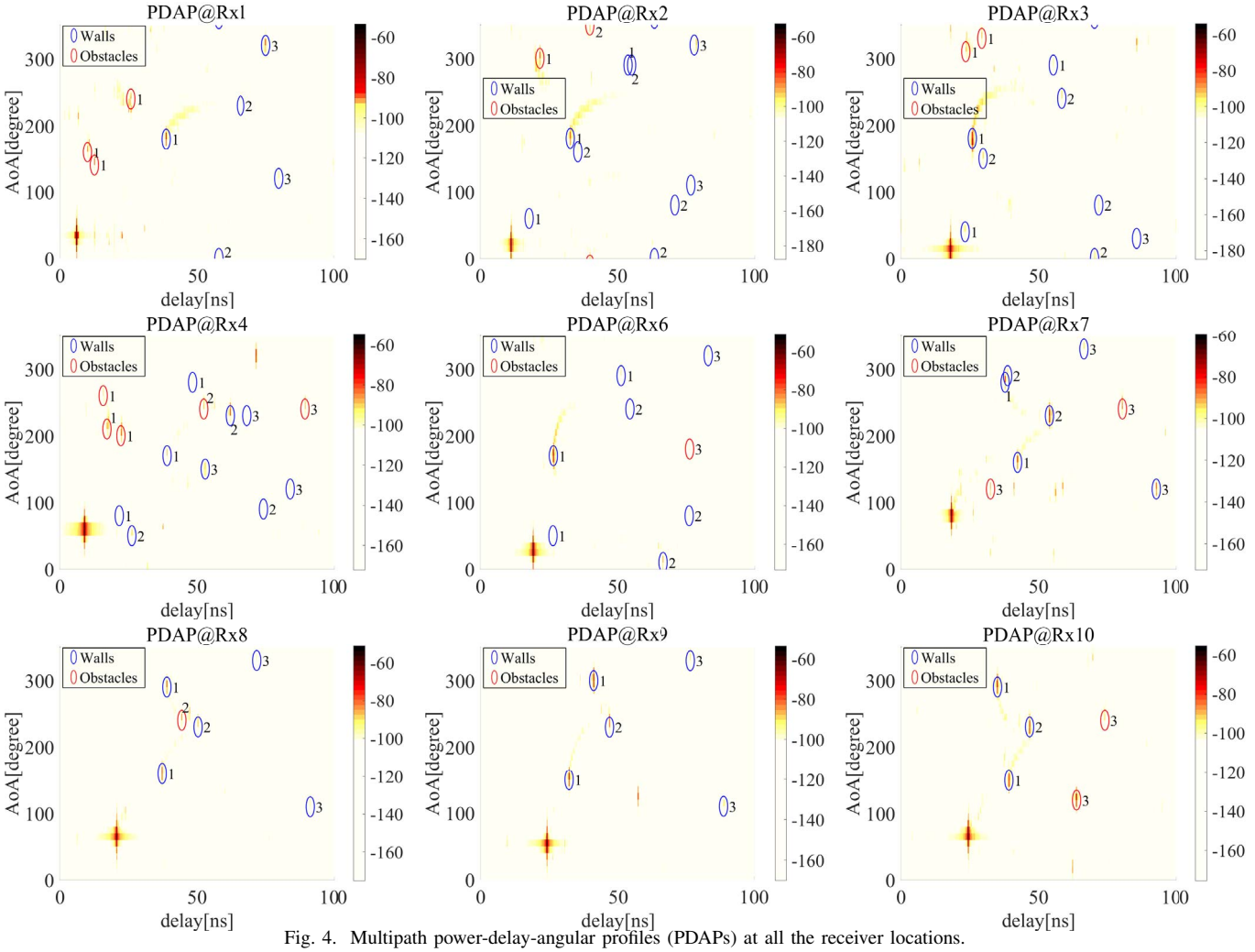

Fig. 4. Multipath power-delay-angular profiles (PDAPs) at all the receiver locations.

B. Multipath Power-Delay-Angular Profiles (PDAPs)

Figure 4 illustrates the multipath *PDAPs* in our measurement campaign, in which the delay and angular profiles for all the measured locations are plotted. A bright point with a tail represents one multipath component (MPC) in the measured THz indoor channel. The resulting multipath effects are dominated by specular reflection of THz waves on object surfaces, including desks, walls, among others. By contrast, attenuation caused by diffusely scattering and diffraction is prohibitively high and excluded in the measurement results [10].

We study the THz reflection below triple interactions since any MPC with more than third-order reflections results in very high path loss and is buried below the background thermal noise. In the indoor environment, we further classify the reflected paths into *wall-reflected* paths and *obstacle-reflected* paths. A wall-reflected path is the one that interacts only with the walls of the meeting room. Otherwise, the reflection belongs to the obstacle-reflected one. The motivation of this classification is that in an extreme case where there are no obstacles like furniture, only wall-reflected paths remain, while reflected MPCs from the ceiling and ground are not considered as they are out of the scope of our equipment. By contrast, the existence of furniture and other obstacles in a room can block some wall-reflected paths while meanwhile produce multiple obstacle-reflected paths.

By simulating the same environment and record the MPCs in ray-tracing algorithm, we can match and thus label the measured paths with various reflection type (wall-reflected or obstacle-reflected) and reflection orders (up to third-order). The labeled reflected paths at each Rx are depicted in Fig. 4. Moreover, the numbers of wall-reflected and obstacle-reflected paths with different reflection orders are computed in Table II and observations are elaborated as follows.

First, the numbers of first-order, second-order, and third-order MPCs for wall reflection in the meeting room that are simulated by the ray-tracing method with omni-directional Tx and Rx are 4, 8, 8, respectively. Due to the directional antenna at Tx, only part of them can be detected by the receivers in our measurements. Second, in general, 2 or 3 first-order wall-reflected paths can be detected at all receivers, except Rx1. This can be explained that Rx1 is very close to the Tx that is located at the corner. Directing the transmission parallel to

a wall, only one first-order back-reflected path is received by Rx1, in addition to the LoS path. Third, the probability of detecting second- and third-order wall-reflected paths is high. The exception is Rx10, which does not receive any third-order wall-reflected path. As a result, we calculate the power ratio between the wall-reflected MPCs and the obstacle-reflected MPCs, $\frac{P_{\text{Wall}}}{P_{\text{other}}}$, which are observed to exceed 0.95. By having this ratio larger than one, one can state that the energy carried by wall-reflected MPCs is higher than that carried by obstacle-reflected MPCs, which further suggests the importance of wall-reflected paths in the environment of THz indoor access networks.

Furthermore, a cumulative density function (CDF) of the path loss of first-order, second-order, and third-order reflected MPCs in our measurement campaign are shown in Fig. 3. By including the propagation and reflection attenuation, the average path loss values of the three kinds are 124.2 dB, 129.5 dB, and 138.6 dB, respectively. Being consistent with intuition, a higher-order reflected path experiences a higher path loss, since it travels through a longer propagation distance and bears larger attenuation from reflection. Indeed, the reflection loss depends on the incident angle, material parameters of objects, and roughness of the reflection surface [10].

C. Temporal and Spatial Features of THz Multipath Propagation

The temporal and spatial distribution are important characteristics of multipath propagation. In Fig. 4, we clearly observe that the MPCs are resolvable in both temporal and angular domains. The background thermal noise occupies most of the region in PDAPs and the number of MPCs is around ten depending on the receiver position. Therefore, the indoor channel at 140 GHz is very *sparse*. The cost of the high directional beam at Tx is that the blockage of the LoS path causes a severe reduction in the THz link performance. Therefore, although with high sparsity and a high K-factor in our scenario, it is not appropriate to neglect the MPCs in channel modeling, which would be significant when the LoS path is blocked since considerable energy is contributed by the NLoS MPCs according to our measurement results.

To characterize the power distribution among all the paths, we first evaluate the *K-factor*, K, which is defined as the ratio between the power of the LoS path and the power of the remaining NLoS MPCs, as computed in Table III. A large K-factor means that the LoS path dominates in the channel. We see that the K-factor ranges from 12.4 dB to 39.57 dB, and swings greatly over varying receiver positions in the room, which implies a very good LoS condition in this scenario. The highest K-factor appears at Rx1, where the propagation distances of reflected MPCs are substantially longer than that of the LoS. For example, two first-order obstacle-reflected paths coming from the desk and chairs are the nearest to the LoS path, which, however, introduces an additional 6 dB free-space path loss since their ToAs are double of the LoS ToA. Meanwhile, the angles-of-departure (AoDs) of the two reflected MPCs are 60° away from the LoS path, which leads to a severe beam misalignment and introduces 30 dB loss. Taking an additional reflection loss, we notice that the received power of the two paths is at least 40 dB lower than the LoS path. To sum up, a longer propagation distance, an additional reflection loss, and beam misalignment of the reflected MPCs are the three critical factors that cause a high K-factor at a receiver.

The power dispersion of MPCs in the temporal domain is quantified by *root-mean-square (RMS) delay spread (DS)*, τ_{rms}, which is calculated as,

$$\tau_{\text{rms}} = \sqrt{\frac{\int_0^\infty (\tau - \bar{\tau})^2 A_c(\tau) d\tau}{\int_0^\infty A_c(\tau) d\tau}} \tag{4}$$

with

$$\bar{\tau} = \frac{\int_0^\infty \tau A_c(\tau) d\tau}{\int_0^\infty A_c(\tau) d\tau} \tag{5}$$

where $A_c(\tau)$ denotes the power angular profile. Similarly, we use *angular spread (AS)* to characterize the power dispersion of MPCs in the spatial domain. The DS and AS of all the measured receivers are listed in Table III. On the one hand, the delay and angular spreads differ among the receivers. However, the deviation is insignificant compared to the metric of K-factor. A small DS value suggests that the received power is confined in the temporal domain, while a small AS value indicates the received power comes from a narrow spatial region, which degrades the spatial degree of freedom.

Specifically, Rx7 has the highest delay spread of 10.02 ns and the largest angular spread of 39.23°. By contrast, the smallest DS equal to 1.17 ns is measured at Rx6. Although these two receivers are far away and reside symmetrically about the diagonal of the meeting room, they have very similar geometry features. First, Rx6 and Rx7 are both at a corner of the meeting room. Second, Rx6, and Rx7 both detect eight reflected MPCs and the composition of their reflected MPCs are very similar (as given in Table II). Third, the difference in the distance from the Tx to the two receivers is only 0.38m. However, Rx6 and Rx7 have substantially different temporal and spatial characteristics, in terms of K-factor, delay spread, and $\frac{P_{\text{Wall}}}{P_{\text{other}}}$. The reason is that there exists a very strong first-order wall-reflected MPC (wall 4) at Rx6 that arrives shortly after the LoS path. Therefore, Rx6 has a small K-factor, large $\frac{P_{\text{Wall}}}{P_{\text{other}}}$, as well as short DS. However, at Rx7, such a wall-reflected MPC (wall 1), which is expected to be strong, is partially obstructed by a metal cabinet. Therefore, all the reflected MPCs are comparable in strengths, and their power is relatively weak compared with the LoS path, which results in high K-factor the power dispersion in the time domain and small $\frac{P_{Wall}}{P_{other}}$. It is seen that the delay spread is highly effected by some critical NLoS MPCs.

D. Correlation among THz Multipath Characteristics

To obtain deep understanding and insights of the THz indoor channel properties, we evaluate the correlations among the temporal and spatial multipath characteristics. In particular, a correlation matrix containing the separation distance among Tx and Rx, the number of MPCs, K-factor, delay

TABLE III
STATISTICS OF MPCS FOR EACH RX.

RX	Distance [m]	K-factor [dB]	DS [ns]	AS [°]
1	1.43	39.57	3.58	25.23
2	3.16	29.07	1.9	20.45
3	5.26	26.14	2.95	33.97
4	2.20	26.65	5.72	20.95
6	5.52	15.96	1.17	26.27
7	5.14	20.07	10.02	39.23
8	5.87	20.38	1.62	16.67
9	6.97	12.60	3.95	29.12
10	7.12	12.40	5.87	31.54

TABLE IV
CORRELATION MATRIX AMONG THZ MULTIPATH CHARACTERISTICS.

	d	N	K	DS	AS	$\frac{P_{\text{Wall}}}{P_{\text{Obstacle}}}$
Distance	1.00	-	-	-	-	-
Number of MPCs	-0.70	1.00	-	-	-	-
K-factor	-0.67	0.02	1.00	-	-	-
Delay spread	0.04	0.00	-0.09	1.00	-	-
Angular Spread	0.37	-0.20	-0.13	0.66	1.00	-
$\frac{P_{\text{Wall}}}{P_{\text{Obstacle}}}$	0.41	-0.42	-0.15	-0.02	0.11	1.00

spread, and angular spread, and the power ratio between wall-reflected and obstacle-reflected MPCs, is presented in Table IV. The main observations are drawn as follows. First, the distance is negatively correlated to the number of paths and K-factor, which suggests that a long separation distance results in a higher channel sparsity and a lower K-factor. This can be explained that if Tx and Rx separate far, the free-space path loss of all the MPCs quadratically increases with the separation distance, while the difference of propagation distance between the LoS and NLoS MPCs decreases. Therefore, for those receiver points far from Tx, MPCs effects are

Moreover, the number of MPCs and K-factor demonstrates no correlation as their correlation coefficient is equal to 0.02. Furthermore, the number of MPCs and K-factor are neither correlated to delay spread nor to angular spread. This suggests that the number of MPCs and K-factor have no impact on the power dispersion in the temporal and spatial domains. Third, the correlation coefficient between delay spread and angular spread is 0.66, which indicates that the temporal and spatial spreads are closely related. This matches with expectation since the power would be likely to disperse in the time domain if it spreads in the spatial domain. However, one interesting observation is that the distance is positively correlated to the angular spread (e.g., the coefficient is 0.37), while it is not much related to the delay spread (e.g., the coefficient is 0.04). This is indeed aligned with our discussions on Rx6 and Rx7 in Sec. III-C, i.e., the two receivers with almost the same separation distance have the smallest and the largest delay spreads, respectively. Fourth, the $\frac{P_{\text{Wall}}}{P_{\text{Obstacle}}}$ illustrates a positive correlation to the distance. Thus, if a receiver is far away from the transmitter, the wall-reflected power needs to be carefully treated, since it contributes significantly to the received power and dominates over other NLoS MPCs.

IV. CONCLUSION

In this paper, we have elaborated extensive channel measurements from 130 GHz to 140 GHz in an indoor meeting room. Ray-tracing techniques are utilized to post-process the received multipath signals. THz channel characterization and analysis are presented, which includes the following insights and lessons.

1) The THz indoor channel is sparse in both temporal and spatial domains, while the number of MPCs is less than 10.
2) Although the transmitter directs a narrow beam to the receiver, the existence of MPCs is still not negligible, especially when receivers are far from Tx.
3) The long propagation distance, additional reflection loss, and beam misalignment of NLoS MPCs cause very a high K-factor and dominant role of the LoS path.
4) Wall-reflected MPCs contain considerably higher power than other obstacle-reflected MPCs in THz indoor environment.
5) Delay spread can be very sensitive NLoS MPCs that arrive shortly after the LoS path, and is positively correlated to angular spread.
6) A longer communication distance might cause a high sparsity, smaller K-factor, broader angular spread, and stronger wall-reflected power.

REFERENCES

[1] I. F. Akyildiz, J. M. Jornet, and C. Han, "Terahertz band: Next frontier for wireless communications," *Physical Communication (Elsevier) Journal*, vol. 12, pp. 16 – 32, Sep. 2014.

[2] C. Han and Y. Chen, "Propagation Modeling for Wireless Communications in the Terahertz Band," *IEEE Commun. Mag.*, vol. 56, no. 6, pp. 96–101, 2018.

[3] S. Priebe, M. Kannicht, M. Jacob, and T. Kurner, "Ultra broadband indoor channel measurements and calibrated ray tracing propagation modeling at THz frequencies," *Journal of Communications and Networks*, vol. 15, no. 6, pp. 547–558, 2013.

[4] S. Kim, W. T. Khan, A. Zajić, and J. Papapolymerou, "D-band channel measurements and characterization for indoor applications," *IEEE Transactions on Antennas and Propagation*, vol. 63, no. 7, pp. 3198–3207, 2015.

[5] B. Peng, S. Rey, and T. Kürner, "Channel characteristics study for future indoor millimeter and submillimeter wireless communications," in *Proc. of 10th European Conference on Antennas and Propagation (EuCAP)*, 2016.

[6] S. Kim and A. Zajić, "Characterization of 300-GHz wireless channel on a computer motherboard," *IEEE Transactions on Antennas and Propagation*, vol. 64, no. 12, pp. 5411–5423, 2016.

[7] N. A. Abbasi, A. Hariharan, A. M. Nair, A. S. Almaiman, F. B. Rottenberg, A. E. Willner, and A. F. Molisch, "Double Directional Channel Measurements for THz Communications in an Urban Environment," *arXiv preprint arXiv:1910.01381*, 2019.

[8] K. Guan, G. Li, T. Kürner, A. F. Molisch, B. Peng, R. He, B. Hui, J. Kim, and Z. Zhong, "On millimeter wave and THz mobile radio channel for smart rail mobility," *IEEE Transactions on Vehicular Technology*, vol. 66, no. 7, pp. 5658–5674, 2016.

[9] Y. Xing and T. S. Rappaport, "Propagation measurement system and approach at 140 GHz-moving to 6G and above 100 GHz," in *Proc. of IEEE Global Communications Conference (GLOBECOM)*, 2018.

[10] C. Han, A. O. Bicen, and I. F. Akyildiz, "Multi-Ray Channel Modeling and Wideband Characterization for Wireless Communications in the Terahertz Band," *IEEE Trans. Wireless Commun.*, vol. 14, no. 5, pp. 2402–2412, 2015.